Photonics and Nanostructures - Fundamentals and Applications 53 (2023) 101094

Contents lists available at ScienceDirect

Photonics and Nanostructures - Fundamentals and Applications

journal homepage: www.elsevier.com/locate/photonics

Polarization-sensitive resonant absorber based on splitted tamm plasmon polariton

A. Yu. Avdeeva [a,*,1], R.G. Bikbaev [a,b,2], S. Ya. Vetrov [a,b,3], R.K. Doyko [b], I.V. Timofeev [a,b,4]

[a] Kirensky Institute of Physics, Krasnoyarsk Scientific Center, Siberian Branch, Russian Academy of Sciences, Krasnoyarsk 660036, Russia
[b] Siberian Federal University, Krasnoyarsk 660041, Russia

ARTICLE INFO

Keywords:
Absorber
Polarization
Localization of light
Tamm plasmon polariton
Anisotropic nanocomposite
Plasmonic sensor

ABSTRACT

The possibility of creating a polarization-sensitive absorber on the basis of the splitting of a Tamm plasmon polariton at the interface between a metallic film and an anisotropic nanocomposite layer conjugated with a photonic crystal is theoretically predicted. The effect of geometrical parameters on the optical absorption spectra under the critical coupling conditions is discussed. It is shown that, changing the polarization of the radiation falling onto the structure along its normal, one can control the absorption at the Tamm plasmon polariton wavelength.

1. Introduction

Tamm plasmon polariton (TPP) is a special electromagnetic surface state in which the field decays exponentially on each side of the surface and energy transfer along the surface can be stopped [1,2]. In contrast to the surface plasmon polariton, such a state can be excited for both s – and p – polarized waves at angles smaller than the total internal reflection angle [3,4]. The TPPs manifest themselves in experiments as narrow resonances in the optical spectrum of a sample at wavelengths within the photonic crystal (PhC) band gap. The TPP phenomenon underlies quite a number of fundamentally new devices, including switches [5], lasers [6,7], white organic light-emitting diodes [8], emitters [9], beem steering [10], sensors [11–13], and optical absorbers [14–17,18]. Optical absorbers have recently attracted particular attention due to their potential for application in solar energy [19,20], sensing [21], thermal radiation [22], visualization [23], and water splitting [24].

To form the TPPs and create devices based on them, planar metallic films conjugated with PhCs are conventionally used. The possibility of optimizing the optical properties of such structures by changing the parameters of a metallic film are limited to the choice of its material and thickness. New opportunities are thin nanocomposite (NC) layers used as structural elements. The effective optical parameters of an NC consisting of metal nanoparticles suspended in a dielectric matrix are caused by the plasmon resonance of nanoparticles and can take unique values in the optical range that are not inherent in natural materials [25–28]. In particular, in [29], we demonstrated the effect of TPP splitting implemented at the interface between a metallic film and an isotropic NC conjugated with a 1D PhC when the resonance frequency of the isotropic NC coincided with the TPP frequency.

Of particular interest are absorbers with the high polarization sensitivity [30]. Therefore, the structures containing optically anisotropic materials are advantageous in designing polarization-sensitive devices [31–33]. These are, for example, anisotropic metal-dielectric NCs, in which the optical anisotropy can be obtained by introducing nanorods [34–37], disks [38], triangular nanoprisms [39,40], or nanocubes [41] into the matrix.

The available technique for manufacturing such materials by self-assembly [42–45–48] makes it possible to align nanoparticles in the only spatial direction and thereby determines the optical properties of obtained NCs. Also, the production of anisotropic NC is possible by stretching glass slabs containing spherical nanoparticles. In particular, this technique is used in commercially available dichroic polarizers, which employ glasses containing elongated silver or copper nanoparticles [49]. The laser-induced anisotropy of the metal nanoparticles

* Corresponding author.
E-mail address: Anastasia-yu-avdeeva@iph.krasn.ru (A.Yu. Avdeeva).
[1] 0000–0002-7609–3755
[2] 0000–0002-0549–5917
[3] 0000–0002-7352–197X
[4] 0000–0002-6558–5607

https://doi.org/10.1016/j.photonics.2022.101094
Received 5 August 2022; Received in revised form 16 November 2022; Accepted 19 November 2022
Available online 24 November 2022

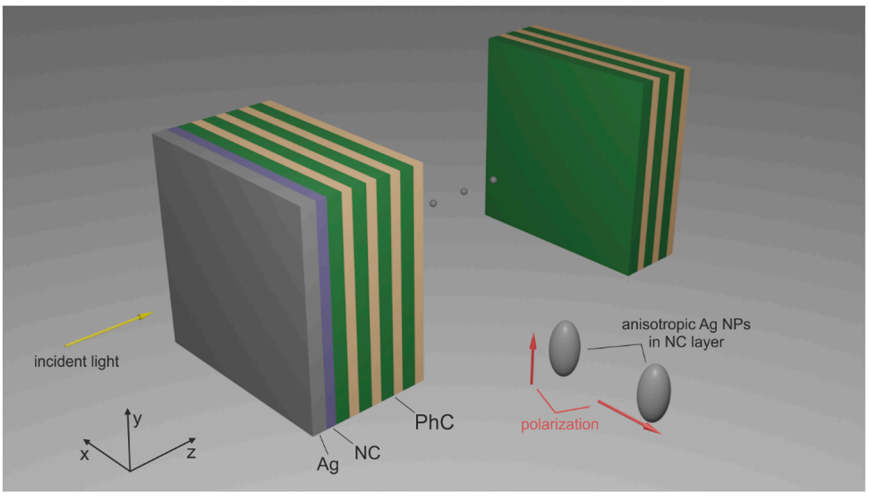

Fig. 1. Schematic of the investigated structure consisting of a silver film, an anisotropic NC and a 1D PhC.

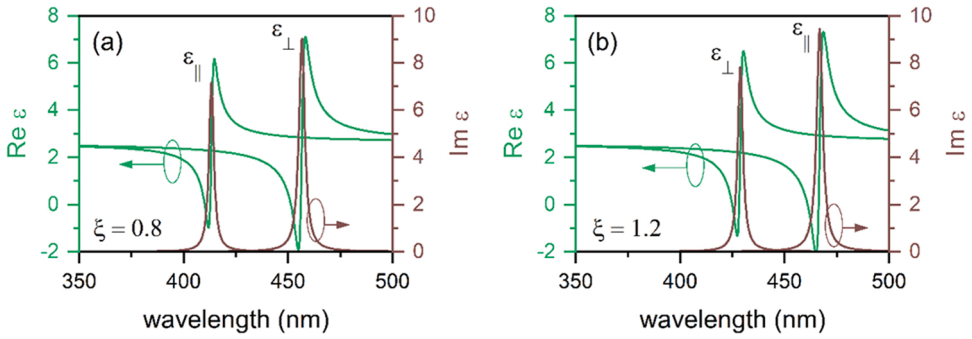

Fig. 2. Real and imaginary parts of the effective permittivities $\varepsilon_{\parallel,\perp}$ as functions of the wavelength, Eq. (1). The NC film parameters are $\varepsilon_d = 2.56$, $\varepsilon_0 = 5$, $\hbar\omega_p = 9eV$, $\hbar\gamma = 0.02eV$ [53],and $f = 1\%$ and aspect ratios ξ between lengths of the polar and equatorial nanoparticle semiaxes are (a) $\xi = 0.8$ and (b) $\xi = 1.2$.

manifests itself in the polarization sensitivity of the optical absorption spectra [50].

In this work, we propose theoretically and demonstrate numerically a polarization-sensitive absorber consisting of a metallic film and an anisotropic NC layer conjugated with a PhC mirror. The features of the frequency splitting of TPPs localized at the interface between two mirrors are presented in dependence on the volume fraction of nanoparticles and aspect ratio between the polar and equatorial semiaxes of the anisotropic NC spheroids, which makes the transmittance spectra polarization-sensitive. The proposed device is expected to be used in optical absorbers, switches, and narrow-band selective filters.

2. Description of the model

Figure 1 shows a schematic of the proposed polarization-sensitive absorber, which consists of a metallic film, an anisotropic NC layer, and a 1D PhC. The PhC unit cell consists of alternating layers of silicon dioxide SiO_2 with a permittivity of $\varepsilon_a = 2.10$ and zirconium dioxide ZrO_2 with a permittivity of $\varepsilon_b = 4.16$ with respective thicknesses d_a and d_b. The lattice period is $L = d_a + d_b$. The number of PhC periods is 12. The metallic film is characterized by permittivity ε_m. The medium surrounding the structure is assumed to be vacuum.

The anisotropic NC layer with thickness d consists of metal nanoparticles in the form of spheroids (ellipsoids of revolution) uniformly distributed over a dielectric matrix and oriented along the rotation axis coinciding with the y axis. The permittivities $\varepsilon_\parallel$ and $\varepsilon_\perp$ are determined using the Maxwell–Garnett model widely used in studying matrix media, in which isolated inclusions are dispersed in a small volume fraction in the matrix material [51]:

$$\varepsilon_{\parallel,\perp}(\omega) = \varepsilon_d\left[1 + \frac{f(\varepsilon_m(\omega) - \varepsilon_d)}{\varepsilon_d + (1-f)(\varepsilon_m(\omega) - \varepsilon_d)L_{\parallel,\perp}}\right], \tag{1}$$

here, f is the filling factor, i.e., the volume fraction of nanoparticles in the matrix, ε_d and $\varepsilon_m(\omega)$ are the permittivities of the matrix and nanoparticle metal, ω is the radiation frequency, and $L_{\parallel,\perp}$ are the depolarization factors depending on the aspect ratio ξ between the lengths of the polar (a) and equatorial (b) spheroid semiaxes and on the field direction. The polar axis is directed along the y axis, the equatorial axis of the nanoparticle is directed along the x axis. For the field directed along the spheroid rotation axis, the factor $L_\parallel$ is expressed as:

$$L_\parallel = \frac{1}{1-\xi^2}\left[1 - \xi\frac{\arcsin\sqrt{1-\xi^2}}{1-\xi^2}\right]. \tag{2}$$

For the field perpendicular to the spheroid rotation axis, we have:

$$L_\perp = (1 - L_\parallel)/2, \tag{3}$$

where $\xi = a/b$. The ξ value is determined by the ratio between the lengths of the polar and equatorial semiaxes of the ellipsoid. At $\xi < 1$, a nanoparticle is an oblate ellipsoid of revolution and, at $\xi > 1$, the elongated one. The case $\xi = 1$ corresponds to the isotropic NC with $L_\perp = L_\parallel = 1/3$ at $\varepsilon_\parallel = \varepsilon_\perp = \varepsilon_{eff}$.

The permittivity of the nanoparticle metal is determined using the Drude–Sommerfeld approximation:

$$\varepsilon_m(\omega) = \varepsilon_0 - \frac{\omega_p^2}{\omega(\omega + i\gamma)}, \tag{4}$$

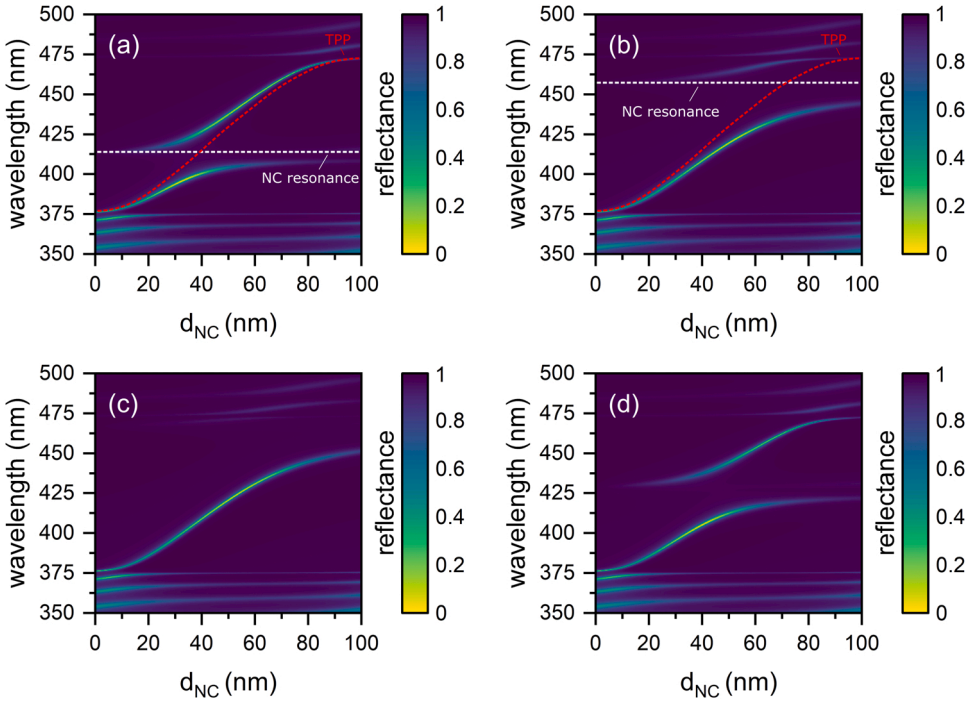

Fig. 3. Reflectance spectrum of the structure vs thickness d at the parallel polarization of light at (a) $\xi = 0.8$ and (c) $\xi = 1.2$ and the perpendicular polarization of light at (b) $\xi = 0.8$ and (d) $\xi = 1.2$ relative to the NC optical axis; $f = 1\%$. The silver layer thickness is 70 nm and the PhC consists of 25 alternating ZrO_2 and SiO_2 layers with $d_a = 74$ nm,$d_b = 50$ nm. White and red dashed lines are shown the NC resonance wavelength and TPP wavelength in the case of $f = 0$, respectively.

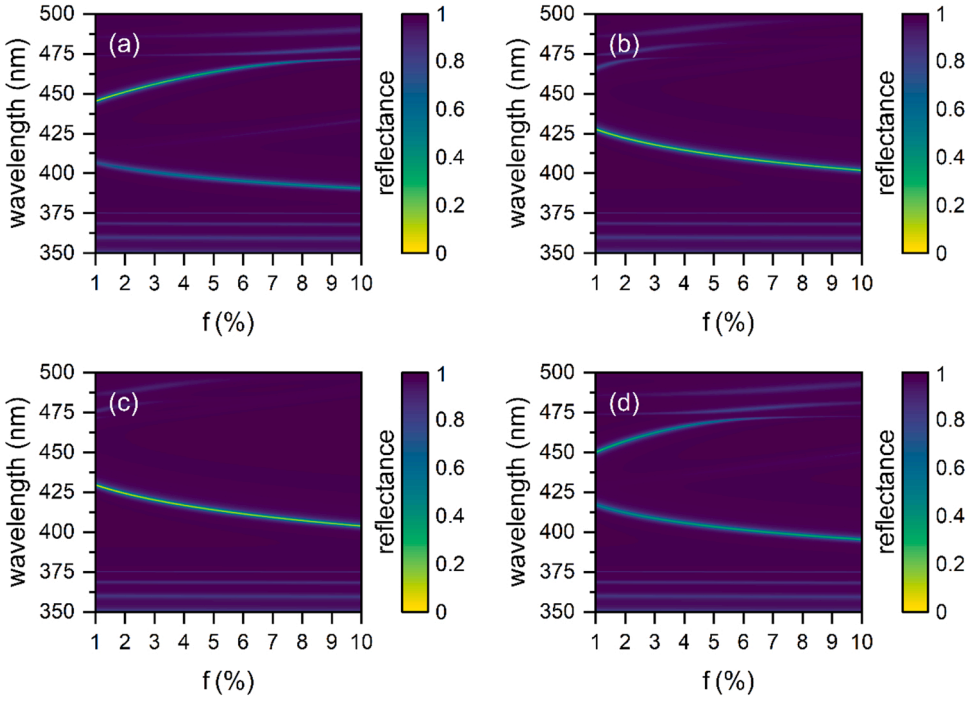

Fig. 4. Reflectance spectra of the structure at different filling factor f at the parallel polarization of light at (a) $\xi = 0.8$ and (c) $\xi = 1.2$ and the perpendicular polarization of light at (b) $\xi = 0.8$ and (d) $\xi = 1.2$ relative to the NC optical axis; $d_{NC} = 50$ nm and other parameters are the same as in Fig. 3.

where ε_0 is the constant taking into account the contributions of interband transitions, ω_p is the plasma frequency, and γ is the reciprocal electron relaxation time.

The $\varepsilon_{\parallel,\perp}(\omega)$ function is complex:

$$\varepsilon_{\parallel,\perp}(\omega) = Re\varepsilon_{\parallel,\perp}(\omega) + iIm(\varepsilon_{\parallel,\perp}(\omega)). \quad (5)$$

The model under study assumes the orientation of all spheroids in one direction, in which case the optical resonances corresponding to the longitudinal and transverse polarizations of ellipsoids can be excited separately, for which it is sufficient to orient the direction of oscillations of the electric field vector of the light wave either along or across the y axis (optical axis of NC). In the case of chaotic orientation of ellipsoids,

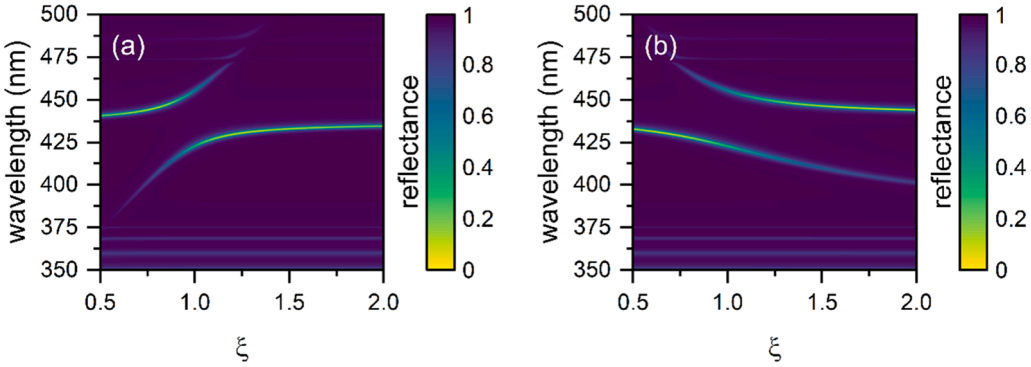

Fig. 5. Reflectance spectrum of the structure vs aspect ratio ξ for (a) the parallel and (b) perpendicular polarization of light relative to the anisotropic NC optical axis; $f = 1$ %, $d_{NC} = 50$ nm, and the rest parameters are as in Fig. 3.

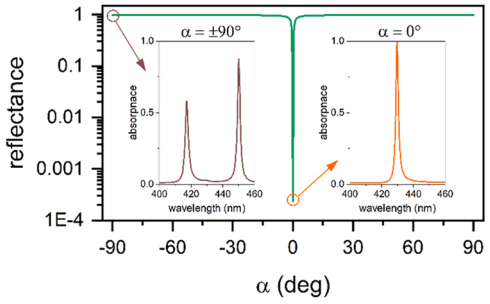

Fig. 6. Reflectance spectra of the structure at $\lambda = 429.5$ nm and different polarization angles α. Insets: absorption spectra of the structure at $\alpha = \pm 90^{\circ}$ (on the left) and $\alpha = 0^{\circ}$ (on the right); $f = 1$ % and $d_{NC} = 50$ nm.

the polarizability of both the longitudinal and transverse polarization of the external light wave will depend simultaneously on both components of the dielectric constant Eq. (1), which will lead to hybridization of resonances [52].

3. Results and discussion

Figures 2a and 2b show the resonance frequency dependences of the real and imaginary parts of the effective permittivity of the anisotropic NC film calculated using Eq. (1) for the oblate (flattened) ellipsoids at $\xi = 0.8$ and prolate (elongated) ellipsoids at $\xi = 1.2$ with a constant filling factor of $f = 1\%$. It can be seen that the resonance frequencies depend on the electric field direction relative to the optical axis of NC and the aspect ratio ξ between the lengths of the polar and equatorial nanoparticle semiaxes. The difference between the resonance frequencies of permittivities $\varepsilon_{\parallel}$ and $\varepsilon_{\perp}$ leads to the dependence of the optical properties of the NC on the polarization of an incident wave.

In particular, for the oblate ellipsoids, the resonances are observed at wavelengths of 413.2 and 456.6 nm, while for the prolate ones, at 466.9 and 428.9 nm. Therefore, depending on the polarization of the incident light, the positions of the anisotropic NC resonances are separated by 43.4 and 38 nm for the oblate and prolate ellipsoidal shapes of metal nanoparticles, respectively. We note that, at the strong anisotropy of the NC ($\xi >> 1$), the plasmon resonances for the field directed along the spheroid axis appear outside the visible range of the spectrum.

Figure 3 presents the comparative reflectance spectra of the proposed structure calculated by the transfer matrix method [54] at different NC layer thicknesses d_{NC} for the oblate particles (Fig. 3a, 3b) and prolate particles (Fig. 3c, 3d). The corresponding geometric parameters of the PhC mirror and metallic film are given in the caption to Figure 3. The red dashed curve corresponds to the TPP wavelength in the case of $f = 0$. As the NC layer thickness d_{NC} changes, the phase of the wave reflected from the PhC changes and the TPP wavelength undergoes a red shift, which makes it possible to tune the TPP position. When the NC layer is filled with metallic silver nanospheroids with the reflectance spectrum reveals the TPP frequency splitting effect (see Fig. 3d). It can be seen in Fig. 3a that, for the oblate ellipsoids with $\varepsilon_{\parallel}$ and $d_{NC} = 50$ nm, the peaks in the reflectance spectrum appear at wavelengths of 406.7 and 445.3 nm; in this case, the TPP splitting value is $\Delta\lambda = 38.6$ nm, while at $d_{NC} = 30$ nm we have $\Delta\lambda = 22.2$ nm. Similarly, for the prolate ellipsoids with $\varepsilon_{\perp}$ and $d = 50$ nm, the reflectance peaks appear at wavelengths of 417.2 and 450 nm (Fig. 3d). At this $\varepsilon_{\perp}$ value and $\xi = 0.8$ (Fig. 3b) for $\varepsilon_{\parallel}$ and at $\xi = 1.2$ (Fig. 3c),the frequencies of the NC resonance are outside the band gap of the PhC; therefore, the TPP does not split and the only Tamm mode is observed in the reflectance spectra within the photonic band gap.

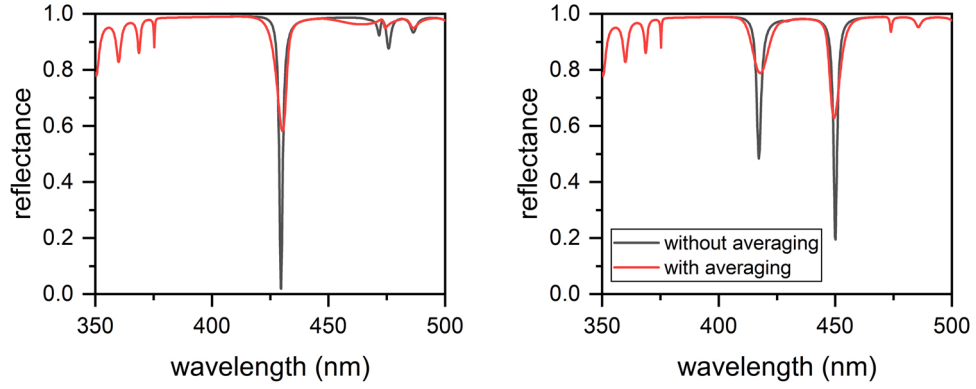

Fig. 7. Reflectance spectra of the investigated structure at the parallel polarization of light (a) and the perpendicular polarization of light (b). The black curves correspond to the case of $\xi = 1.2$, the red curves are obtained taking into account the averaging of ξ from 0.9 to 1.5. The rest parameters are the same as in Fig. 5.

Figure 4 shows the NC nanoball concentration effect on the reflectance spectrum. We consider the comparative reflectance spectra of the structure under study at different volume fractions of nanoparticles in the NC layer at concentrations from 1 % to 10 %. It can be clearly seen in Figs. 4a and 4d that, in these two cases, upon variation in the filling factor f, the high- and low-frequency modes are anti-crossed symmetrically and the splitting value increases with the concentration of silver nanoballs in the NC layer. In particular, for $\varepsilon_{\parallel}$ at $f = 0.05$ and $\xi = 0.8$, Fig. 4a shows that the TPP splits into two Tamm modes: the high-Q mode $\lambda_1 = 396.8$ nm and the low-Q mode $\lambda_2 = 463.6$ nm; therefore, the TPP splitting value is $\Delta\lambda = 66.8$ nm, which is twice as much as the splitting value at a concentration of 1%. Similarly, for $\varepsilon_{\perp}$ at $f = 0.05$ and $\xi = 1.2$, Fig. 4d shows that the TPP splits into two Tamm modes, $\lambda_1 = 403.4$ nm and $\lambda_2 = 469.2$ nm. In the other two cases illustrated in Figs. 4b and 4c, the only high-Q Tamm mode is observed in the reflectance spectrum of the structure under study.

Note that a decrease in the number of periods of the dielectric mirror can lead to a significant decrease in the Q-factor of the split peaks. So, for the case of flattened ellipsoids, at $\xi = 0.8$, the Q-factor of the high-frequency reflection peak at 10 periods decreases by 10 % compared to 12 periods, and at 8 periods the Q-factor of the peak decreases by 40 %. At the same time, an increase in periods does not lead to a significant increase in the Q-factor of peaks. Thus, to demonstrate the effects we have obtained, we have proposed the optimal number of periods of the dielectric mirror to ensure Q-factor is high enough to resolve coupled spectral peaks in strong mode coupling [55].

In the investigated structure, the change not only in the filling factor f, but also in aspect ratio ξ leads to a change in the positions of the Tamm modes. Figure 5 shows the positions of the resonance reflection peaks for both light polarization directions relative to the anisotropic NC optical axis.The ξ parameter varied from 0.5 to 2 in order to demonstrate the effect of anisotropy in the case of compression and stretching of the nanoparticle by a factor of two. Note that the choice of mutually inverse values of ξ will not give the symmetry of the observed effect, because $L_{\perp}$ and $L_{\parallel}$ are not exactly exchanged according to Eq. (2), (3). Besides, with an increase in the ξ, the resonance frequency for $\varepsilon_{\parallel}$ shifts to the low-frequency region of the spectrum. In the case of an increase in the ξ and for $\varepsilon_{\perp}$, the resonance frequency shifts to the high-frequency region of the spectrum (see Fig. 2.).

It can be seen that for the parallel permittivity component (Fig. 5a), the intensity of the interaction lowers with an increase in the aspect ratio ξ between the semi-axes, which leads to merging of the TPP, while for the perpendicular permittivity component, the process occurs, which enhances the interaction and leads to subsequent formation of two reflection lines in the PhC band gap.

It should be noted that the TPP splitting corresponding to each of the two orthogonal polarizations of the incident wave can be implemented even at large aspect ratios ξ between the lengths of the ellipsoid semi-axes. To do that, one should change the PhC lattice period, i.e., the position of the PhC band gap relative to the resonance frequencies of the anisotropic NC.

According to the results of the simulation, the change in the volume concentration and shape of nanoparticles in the bulk of the NC film, as well as in its thickness, is an effective way to control the TPP wavelength in the PhC band gap. It is known well that the reflectivity at the TPP wavelengths is determined by the critical coupling condition. Since due to the large number of periods of the photonic crystal the transmittance inside the band gap is zero, the critical coupling condition is met at the equal rates of the energy leakage into the transmission channel of the metallic film and the channel of its absorption. In other words, the critical coupling conditions can be established by changing the thickness of the metallic film. Meanwhile, the calculation shows that, for the NC film with $f = 1$ %, $d_{NC} = 50$ nm, and $\xi = 1.2$, at the parallel orientation of the electric field relative to the NC optical axis, the condition of the critical coupling of the incident field with the TPP is met at a metallic film thickness of $d_M = 67$ nm. The calculated reflectance spectra of the structure at a wavelength of 429.5 nm at different angles α between the NC optical axis and the electric field of the incident light at such a film thickness are shown in Fig. 6. It can be seen that, at $\alpha = 0^{\circ}$ (the electric field is parallel to the NC optical axis), the reflection from the structure is less than 0.1 %. This means that the radiation incident at this wavelength is completely absorbed by the structure. It is attractive that the smooth clockwise or counterclockwise rotation of the electric field vector leads to a sharp increase in the reflection at a specified wavelength and, consequently, to a decrease in the absorption coefficient. The insert in Fig. 6 (on the left) shows the absorptance spectra of the structure for the electric field perpendicular to the NC optical axis. One can see that the absorption coefficient at 429.5 nm is close to zero.

It should be noted that when creating elongated nanoparticles, deviations from the exact geometry of ellipsoids are observed [42]. Fig. 7 shows the reflection spectra of the structure under study in the case when the aspect ratio of the particles ξ is given by normal distribution with $\xi_0 = 1.2$, $\sigma = 0.1$ in the 3σ range from 0.9 to 1.5. It can be seen that, compared with a structure with a fixed $\xi = 1.2$, the Q-factor of the peaks decreases.

Thus, changing the $s-$ and $p-$ polarization of the radiation incident normally onto the structure, one can control the absorption at the TPP wavelength from 2% to 100%. The proposed structure can be used as a perfect polarization-sensitive absorber. It was shown that the proposed absorption efficiency is mainly determined by the concentration and orientation of nanoparticles and its working wavelength can be controlled by changing the NC layer thickness. The combination of the above parameters makes a strong impact on the absorption bandwidth and Q-factor of the absorber. The results obtained can be a good guideline for the experimental design.

4. Conclusions

The polarization-sensitive absorber based on the splitting of a Tamm plasmon polariton at the interface between a metallic mirror and an anisotropic nanocomposite conjugated with a superlattice was proposed theoretically and demonstrated numerically. It was shown that the absorption at the Tamm plasmon polariton wavelength can be tuned up to 100 % in the visible light range by changing the polarization of the radiation falling onto the structure along its normal. The results obtained allowed us to conclude that the use of ellipsoidal nanoparticles offers more opportunities for frequency tuning of the spectrum than the use of spherical particles. The proposed absorber is a candidate for designing anisotropic devices with tunable spectra and selective polarization in the visible light range.

Declaration of Competing Interest

The authors declare that they have no known competing financial interests or personal relationships that could have appeared to influence the work reported in this paper.

Data availability

Data will be made available on request.

References

[1] M. Kaliteevski, I. Iorsh, S. Brand, R.A. Abram, J.M. Chamberlain, A.V. Kavokin, I. A. Shelykh, Tamm plasmon-polaritons: possible electromagnetic states at the interface of a metal and a dielectric bragg mirror, Phys. Rev. B 76 (16) (2007).

[2] M.E. Sasin, R.P. Seisyan, M.A. Kalitteevski, S. Brand, R.A. Abram, J. M. Chamberlain, A. Yu. Egorov, A.P. Vasil'ev, V.S. Mikhrin, A.V. Kavokin, Tamm plasmon polaritons: slow and spatially compact light, Appl. Phys. Lett. 92 (25) (2008), 251112.

[3] Alexey Kavokin, Ivan Shelykh, Guillaume Malpuech, Optical tamm states for the fabrication of polariton lasers, Appl. Phys. Lett. 87 (26) (2005), 261105.

[4] H. Ohno, E.E. Mendez, J.A. Brum, J.M. Hong, F. Agulló-Rueda, L.L. Chang, L. Esaki, Observation of "tamm states" in superlattices, Phys. Rev. Lett. 64 (21) (1990) 2555–2558.

[5] W.L. Zhang, S.F. Yu, Bistable switching using an optical tamm cavity with a kerr medium, Opt. Commun. 283 (12) (2010) 2622–2626.

[6] C. Symonds, A. Lema\relax \special {t4ht=1}ˆtre, P. Senellart, M.H. Jomaa, S. Aberra Guebrou, E. Homeyer, G. Brucoli, J. Bellessa, Lasing in a hybrid GaAs/silver tamm structure, Appl. Phys. Lett. 100 (12) (2012), 121122.

[7] Wen-Hui Xu, Yu-Hsun Chou, Zih-Ying Yang, Yi-Yun Liu, Min-Wen Yu, Chen-Hang Huang, Chun-Tse Chang, Chen-Yu Huang, Tien-Chang Lu, Tzy-Rong Lin, Kuo-Ping Chen, Tamm plasmon-polariton ultraviolet lasers, Adv. Photonics Res. 3 (1) (2021), 2100120.

[8] Xu-Lin Zhang, Jing Feng, Xiao-Chi Han, Yue-Feng Liu, Qi-Dai Chen, Jun-Feng Song, Hong-Bo Sun, Hybrid tamm plasmon-polariton/microcavity modes for white top-emitting organic light-emitting devices, Optica 2 (6) (2015) 579.

[9] Zih ying Yang, Satoshi Ishii, Takahiro Yokoyama, Thang Duy Dao, Mao guo Sun, Tadaaki Nagao, Kuo ping Chen, Tamm plasmon selective thermal emitters, Opt. Lett. 41 (19) (2016) 4453.

[10] Rashid G. Bikbaev, Dmitrii N. Maksimov, Kuo-Ping Chen, Ivan V. Timofeev, Double-resolved beam steering by metagrating-based tamm plasmon polariton, Materials 15 (17) (2022) 6014.

[11] Partha Sona Maji, Mukesh Kumar Shukla, Ritwick Das, Blood component detection based on miniaturized self-referenced hybrid tamm-plasmon-polariton sensor, Sens. Actuators B: Chem. 255 (2018) 729–734.

[12] Guang Lu, Feng Wu, Minjia Zheng, Chaoxin Chen, Xiachen Zhou, Chao Diao, Fen Liu, Guiqiang Du, Chunhua Xue, Haitao Jiang, Hong Chen, Perfect optical absorbers in a wide range of incidence by photonic heterostructures containing layered hyperbolic metamaterials, Opt. Express 27 (4) (2019) 5326–5336.

[13] Alexandre Juneau-Fecteau, Rémy Savin, Abderraouf Boucherif, Luc G. Fréchette, A practical tamm plasmon sensor based on porous si, AIP Adv. 11 (6) (2021), 065305.

[14] Jiaju Wu, Feng Wu, Chunhua Xue, Zhiwei Guo, Haitao Jiang, Yong Sun, Yunhui Li, Hong Chen, Wide-angle ultrasensitive biosensors based on edge states in heterostructures containing hyperbolic metamaterials, Opt. Express 27 (17) (2019) 24835–24846.

[15] Rashid G. Bikbaev, Stepan Ya. Vetrov, Ivan V. Timofeev, Epsilon-near-zero absorber by tamm plasmon polariton, Photonics 6 (1) (2019).

[16] Feng Wu, Xiaohu Wu, Shuyuan Xiao, Guanghui Liu, Hongju Li, Broadband wide-angle multilayer absorber based on a broadband omnidirectional optical tamm state, Opt. Express 29 (15) (2021) 23976–23987.

[17] Sayed Elshahat, Israa Abood, Mohamed Saleh M. Esmail, Zhengbiao Ouyang, Cuicui Lu, One-dimensional topological photonic crystal mirror heterostructure for sensing, Nanomaterials 11 (8) (2021).

[18] Feng Wu, Ying Chen, Yang Long, Guanghui Liu, Hanying Deng, Hongju Li, Polarization-sensitive optical tamm state and its application in polarization-sensitive absorption, Results Phys. 40 (2022), 105818.

[19] Zhengqi Liu, Haozong Zhong, Guiqiang Liu, Xiaoshan Liu, Yan Wang, Junqiao Wang, Multi-resonant refractory prismoid for full-spectrum solar energy perfect absorbers, Opt. Express 28 (21) (2020), 31763.

[20] Rashid G. Bikbaev, Dmitrii A. Pykhtin, Stepan Ya. Vetrov, Ivan V. Timofeev, Vasily F. Shabanov, Nanostructured photosensitive layer for tamm-plasmon-polariton-based organic solar cells, Appl. Opt. 61 (17) (2022) 5049.

[21] Wei Li, Jason Valentine, Metamaterial perfect absorber based hot electron photodetection, Nano Lett. 14 (6) (2014) 3510–3514.

[22] Franziska B. Barho, Fernando Gonzalez-Posada, Mario Bomers, Aude Mezy, Laurent Cerutti, Thierry Taliercio, Surface-enhanced thermal emission spectroscopy with perfect absorber metasurfaces, ACS Photonics 6 (6) (2019) 1506–1514.

[23] Andreas Tittl, Ann-Katrin U. Michel, Martin Schäferling, Xinghui Yin, Behrad Gholipour, Long Cui, Matthias Wuttig, Thomas Taubner, Frank Neubrech, Harald Giessen, A switchable mid-infrared plasmonic perfect absorber with multispectral thermal imaging capability, Adv. Mater. 27 (31) (2015) 4597–4603.

[24] Maxim Pyatnov, Rashid Bikbaev, Ivan Timofeev, Ilya Ryzhkov, Stepan Vetrov, Vasily Shabanov, Broadband tamm plasmons in chirped photonic crystals for light-induced water splitting, Nanomaterials 12 (6) (2022) 928.

[25] Vasily Klimov, Nanoplasmonics, Jenny Stanford Publishing, 2014.

[26] Anatolii N. Oraevsky, I.E. Protsenko, Optical properties of heterogeneous media, Quantum Electron. 31 (3) (2001) 252–256.

[27] S.V. Sukhov, Nanocomposite material with the unit refractive index, Quantum Electron. 35 (8) (2005) 741–744.

[28] Sergey G. Moiseev, Active maxwell-garnett composite with the unit refractive index, Phys. B: Condens. Matter 405 (14) (2010) 3042–3045.

[29] Anastasia Yu. Avdeeva, Stepan Ya. Vetrov, Ivan V. Timofeev, Splitting of a tamm plasmon polariton at the interface between a metal and a resonant nanocomposite layer conjugated with a photonic crystal, J. Opt. Soc. Am. B 38 (6) (2021) 1792.

[30] A. Polyakov, S. Cabrini, S. Dhuey, B. Harteneck, P.J. Schuck, H.A. Padmore, Plasmonic light trapping in nanostructured metal surfaces, Appl. Phys. Lett. 98 (20) (2011), 203104.

[31] Ai-Li Cao, Kun Zhang, Jia-Rui Zhang, Yan Liu, Wei-Jin Kong, Actively tunable polarization-sensitive multiband absorber based on graphene, Chin. Phys. B 29 (11) (2020), 114205.

[32] Gui Jin, Tianle Zhou, Bin Tang, Ultra-narrowband anisotropic perfect absorber based on α-MoO3 metamaterials in the visible light region, Nanomaterials 12 (8) (2022) 1375.

[33] Daria Ignatyeva, Pavel Kapralov, Polina Golovko, Polina Shilina, Anastasiya Khramova, Sergey Sekatskii, Mohammad Nur-E-Alam, Kamal Alameh, Mikhail Vasiliev, Andrey Kalish, Vladimir Belotelov, Sensing of surface and bulk refractive index using magnetophotonic crystal with hybrid magneto-optical response, Sensors 21 (6) (2021) 1984.

[34] Nikhil R. Jana, Latha Gearheart, Catherine J. Murphy, Wet chemical synthesis of high aspect ratio cylindrical gold nanorods, J. Phys. Chem. B 105 (19) (2001) 4065–4067.

[35] Mahmoud A. Mahmoud, Mostafa A. El-Sayed, Jianping Gao, Uzi Landman, High-frequency mechanical stirring initiates anisotropic growth of seeds requisite for synthesis of asymmetric metallic nanoparticles like silver nanorods, Nano Lett. 13 (10) (2013) 4739–4745.

[36] Michael J.A. Hore, Amalie L. Frischknecht, Russell J. Composto, Nanorod assemblies in polymer films and their dispersion-dependent optical properties, ACS Macro Lett. 1 (1) (2011) 115–121.

[37] Robert C. Ferrier, Jason Koski, Robert A. Riggleman, Russell J. Composto, Engineering the assembly of gold nanorods in polymer matrices, Macromolecules 49 (3) (2016) 1002–1015.

[38] Jun Yang, Qingbo Zhang, Jim Yang Lee, Heng-Phon Too, Dissolution-recrystallization mechanism for the conversion of silver nanospheres to triangular nanoplates, J. Colloid Interface Sci. 308 (1) (2007) 157–161.

[39] Rongchao Jin, Yun Wei Cao, Chad A. Mirkin, K.L. Kelly, George C. Schatz, J. G. Zheng, Photoinduced conversion of silver nanospheres to nanoprisms, Science 294 (5548) (2001) 1901–1903.

[40] Jill E. Millstone, Sungho Park, Kevin L. Shuford, Lidong Qin, George C. Schatz, Chad A. Mirkin, Observation of a quadrupole plasmon mode for a colloidal solution of gold nanoprisms, J. Am. Chem. Soc. 127 (15) (2005) 5312–5313.

[41] Matthew Rycenga, Joseph M. McLellan, Younan Xia, Cover picture: controlling the assembly of silver nanocubes through selective functionalization of their faces (adv. mater. 12/2008), Adv. Mater. 20 (12) (2008).

[42] H. Hofmeister, W.-G. Drost, A. Berger, Oriented prolate silver particles in glass – characteristics of novel dichroic polarizers, Nanostruct. Mater. 12 (1–4) (1999) 207–210.

[43] Michael B. Ross, Martin G. Blaber, George C. Schatz, Using nanoscale and mesoscale anisotropy to engineer the optical response of three-dimensional plasmonic metamaterials, Nat. Commun. 5 (1) (2014).

[44] Matthew R. Jones, Kyle D. Osberg, Robert J. Macfarlane, Mark R. Langille, Chad A. Mirkin, Templated techniques for the synthesis and assembly of plasmonic nanostructures, Chem. Rev. 111 (6) (2011) 3736–3827.

[45] Matthew R. Jones, Robert J. Macfarlane, Byeongdu Lee, Jian Zhang, Kaylie L. Young, Andrew J. Senesi, Chad A. Mirkin, DNA-nanoparticle superlattices formed from anisotropic building blocks, Nat. Mater. 9 (11) (2010) 913–917.

[46] Qingkun Liu, Yanxia Cui, Dennis Gardner, Xin Li, Sailing He, Ivan I. Smalyukh, Self-alignment of plasmonic gold nanorods in reconfigurable anisotropic fluids for tunable bulk metamaterial applications, Nano Lett. 10 (4) (2010) 1347–1353.

[47] Xingchen Ye, Jun Chen, Michael Engel, Jaime A. Millan, Wenbin Li, Liang Qi, Guozhong Xing, Joshua E. Collins, Cherie R. Kagan, Ju Li, Sharon C. Glotzer, Christopher B. Murray, Competition of shape and interaction patchiness for self-assembling nanoplates, Nat. Chem. 5 (6) (2013) 466–473.

[48] Kaylie L. Young, Matthew R. Jones, Jian Zhang, Robert J. Macfarlane, Raul Esquivel-Sirvent, Rikkert J. Nap, Jinsong Wu, George C. Schatz, Byeongdu Lee, Chad A. Mirkin, Assembly of reconfigurable one-dimensional colloidal superlattices due to a synergy of fundamental nanoscale forces, Proc. Natl. Acad. Sci. USA 109 (7) (2012) 2240–2245.

[49] A. Berger, W.G. Drost, S. Hopfe, M. Steen, H. Hofmeister, Stress state and twin configuration of spheroidal silver nanoparticles in glass. Nanostructured and Advanced Materials for Applications in Sensor, Optoelectronic and Photovoltaic Technology, Springer, Netherlands, 2022, pp. 323–326.

[50] Andrei Stalmashonak, Gerhard Seifert, Amin Abdolvand, Ultra-Short Pulsed Laser Engineered Metal-Glass Nanocomposites, Springer International Publishing, 2013.

[51] A. Sihvola.Electromagnetic mixing formulas and applications. Number 47 in Electromagnetic Waves Series. Institute of Electrical Engineers, United Kingdom, 1999.

[52] S.G. Moiseev, Nanocomposite-based ultrathin polarization beamsplitter, Opt. Spectrosc. 111 (2) (2011) 233–240.

[53] P.B. Johnson, R.W. Christy, Optical constants of the noble metals, Phys. Rev. B 6 (12) (1972) 4370–4379.

[54] Yeh Pochi, Electromagnetic propagation in birefringent layered media, J. Opt. Soc. Am. 69 (5) (1979) 742.

[55] Mikhail V. Rybin, Mikhail F. Limonov, Resonance effects in photonic crystals and metamaterials (100th anniversary of the ioffe institute), Uspekhi Fiz. Nauk 189 (08) (2019) 881–898.